Fibrils or Globules? Tuning the Morphology of Peptide Aggregates from Helical Building Blocks

ARTICLE *in* THE JOURNAL OF PHYSICAL CHEMISTRY B · APRIL 2013

Impact Factor: 3.3 · DOI: 10.1021/jp400009j · Source: PubMed

THE JOURNAL OF PHYSICAL CHEMISTRY B

Article

pubs.acs.org/JPCB

Fibrils or Globules? Tuning the Morphology of Peptide Aggregates from Helical Building Blocks

M. Caruso,[†] E. Placidi,[‡,§] E. Gatto,[†] C. Mazzuca,[†] L. Stella,[†] G. Bocchinfuso,[†] A. Palleschi,[†] F. Formaggio,[∥] C. Toniolo,[∥] and M. Venanzi*[,†]

[†]Dipartimento di Scienze e Tecnologie Chimiche and [‡]Dipartimento di Fisica, Università di Roma 'Tor Vergata', 00133 Roma, Italy

[§]Istituto di Struttura della Materia, CNR, 00133 Roma, Italy

[∥]ICB, Padova Unit, CNR, Dipartimento di Scienze Chimiche, Università di Padova, Padova, Italy

Supporting Information

ABSTRACT: The aggregation propensity of helical oligopeptides formed exclusively by the conformationally constrained α-aminoisobutyric acid (Aib or U in a three- or single-letter code, respectively) was studied in methanol and methanol/water solutions by spectroscopic methods (UV−vis absorption, steady-state and time-resolved fluorescence, and FT-IR absorption) and atomic force microscopy (AFM) imaging. The peptides investigated have the general formula U_nN, where n = 6, 12, and 15 and N stands for a naphthyl chromophore introduced with the dual aim to serve as a spectroscopic probe and to analyze the effect of an extended aromatic group on the aggregation process. Experiments showed that the aggregation propensity in $(70/30)_{v/v}$ and $(50/50)_{v/v}$ methanol/water solutions increases with increasing the length of the peptide chain, i.e., $U_6N < U_{12}N < U_{15}N$. When the peptides are immobilized on mica as a dried film, the interplay of aromatic−aromatic and interhelix interactions, the latter becoming more and more important with the elongation of the peptide chain, governs the morphology of the resulting mesoscopic aggregates. AFM imaging revealed the formation of globular or fibrillar structures, the predominance of which is controlled by the helix length of the peptide building block.

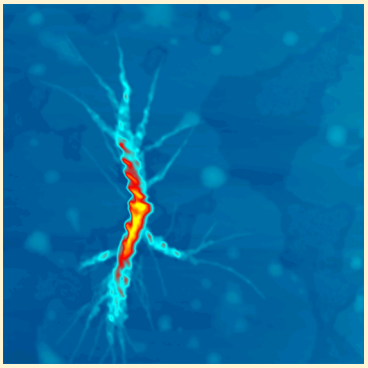

INTRODUCTION

Peptides are currently finding interesting applications as versatile building blocks for the design of novel smart materials in bioinspired nanotechnology.[1] Nanosensors,[2] molecular photodiodes,[3] and biocompatible platforms for tissue engineering[4] have been successfully developed using peptides as elementary units. In materials science the use of natural peptides has been rapidly substituted by a sort of peptide LEGO, made possible by the impressive progress that peptide and peptidomimetic chemistries realized in the past decade.[5] Well-established protocols to synthesize peptide compounds of controlled secondary structures and endowed with specific functions are now commonly adopted.

Self-assembly, i.e., the spontaneous organization of molecular components in an ordered structure, has been the strategy of choice for building nano- and mesoscopic structures from single peptide elements.[6] Indeed, formation of molecular architectures with nanometric order is the demanding requirement of most nanotechnology processes. In this framework, using peptides populating specific secondary structures could represent the most direct approach to this goal.[7]

Bioinspired self-assembly, however, is driven by the full spectrum of interactions, from strong electrostatic forces to an ensemble of weak interactions, i.e., van der Waals, H-bonding, and hydrophobic effects.[8] In this regard, specific interactions between aromatic groups may assume a major role in determining the final morphology of the aggregates. This aspect is of particular relevance in the study of the early stages of formation of amyloids,[9] peptide aggregates that are responsible for a series of neurological degenerative pathologies (Alzheimer, Parkinson, and Creutzfeld-Jacob diseases and type-II diabetes).[10]

The dependence of such processes on the peptide composition and sequence is now well established.[11] In the case of Alzheimer disease, two peptides were identified as capable of giving rise to amyloid fibrillization, i.e., Aβ(1−40) and Aβ(1−42). In particular, the sequence KLVFF (Aβ16−20), characterized by the -Phe-Phe- (FF) motif, was shown to be the key element promoting aggregation.[12] Formation of fibrils is thought to proceed through a two-step pathway: (i) formation of small spherulites, a very fast process corresponding to nucleation and (ii) a relatively slow growth of fibrillar structures.[13] This second step is strongly dependent on the peptide secondary structure. In the case of β-lactoglobulin, rich in β-sheet structures, the aggregation is very fast, whereas for lysozyme (30−40% of helical sequences), fibril formation occurs with a time lag of 48 h. All of these processes are strongly dependent on peptide concentration. Higher concen-

Received: January 1, 2013
Revised: March 13, 2013
Published: April 12, 2013

   dx.doi.org/10.1021/jp400009j | J. Phys. Chem. B 2013, 117, 5448−5459

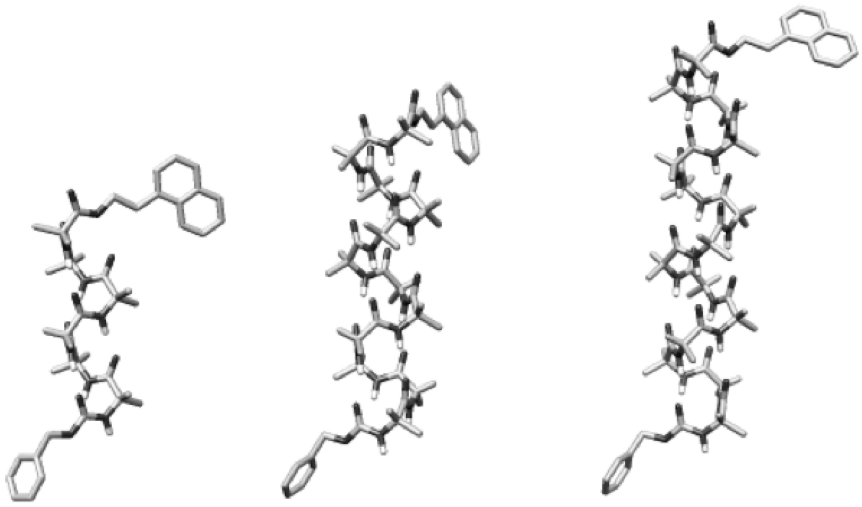

Figure 1. Stick representations of the peptides investigated. From left to right: U_6N (3_{10}-helix), $U_{12}N$ (α-helix), and $U_{15}N$ (α-helix). Note the C-terminal naphthyl chromophore on top and the benzyloxycarbonyl group at the N-terminus.

tration implies a larger number of seeds, faster aggregation, and, usually, shorter fibrils.[8,14]

In such a context, the role of aromatic−aromatic interactions is crucial for determining the morphology of the aggregates. Peptide analogues comprising several FF repeats have been shown to form globular structures, nanotubes, or fibrils depending on the experimental conditions.[15] Furthermore, it was found that, by substituting a Phe residue with Leu, aggregation is only partially suppressed, but it is completely depleted in the case of substitution with the much less hydrophobic Ala residue. The latter is a well-known helicogenic amino acid, but its tendency to form β-sheets, the typical seed of growth of fibrillar structures, is definitely lower.[16]

Homo-oligopeptides are suitable models for our understanding of the basic mechanisms driving aggregation. They are simple enough to allow one to investigate the details of aggregation at a molecular level, but they still retain sufficient complexity to give rise to a rich morphology of aggregated structures (nanotubes, wires, and fibrils) depending on the operative experimental conditions (pH, concentration, and ionic strength).[17] V_6D, A_6K, and G_8DD[18] were shown to form nanotubes of 30−50 nm diameter and micrometric length. Recently, Hauser et al.[19] demonstrated that short linear peptides with 3−7 aliphatic amino acids are able to self-assemble into helical fibers, giving rise to mesoscopic structures with high mechanical stiffness, thermal stability, and biocompatibility.

Besides enhancing hydrophobic effects in aqueous solutions, aromatic−aromatic interactions can modulate the morphology of supramolecular structures forming specifically oriented aggregates. J-aggregates, i.e., end-to-end displaced stacked dimers, are characterized by a bathochromic shift of the UV−vis absorption spectra and an intense fluorescence emission, whereas H-aggregates, i.e., sandwiched stacked dimers, are generally recognized by a blue shift of the absorption spectrum (hypsochromism) and a very low-intensity fluorescence.[20] Excited-state complexes may give rise, under appropriate conditions, to a red-shifted broad emission (excimers).[21]

The target of this study are model homo-oligopeptides comprising exclusively α-aminoisobutyric acid residues (denoted as Aib or U in a three- or single-letter code notation, respectively) of general formula U_nN, with n = 6, 12, and 15 (Figure 1). N indicates a naphthyl group which functionalizes the peptide chain at the C-terminus. It plays the dual role of being a fluorescent probe and a bicyclic aromatic group influencing the aggregation properties of the compounds examined. Benzyloxycarbonyl (Z) is a well-known protective group, widely employed in peptide chemistry for its stability (it is almost insensitive to light, heat or pH changes) and easy removal (H_2, catalyst). Furthermore, its aromatic group allows to easily follow the reaction progress by TLC. Regarding the secondary structure attained by the peptide chain, extensive IR and NMR investigations did not reveal substantial differences with respect to other protective groups (Boc, Fmoc, ...). However, Z increases the hydrophobicity of the peptide chain and promotes peptide aggregation in aqueous solutions. Aib homo-oligopeptides are well-known to populate 3_{10}- or α-helical conformations depending on the length of the sequence, as confirmed by X-ray diffraction studies on peptide crystals and NMR experiments in solution.[5,22] A statistical analysis carried out on the crystal structures of 57 globular proteins revealed the presence of 71 3_{10}-helices of length comprised between 3 and 6 residues, most of which found at the N- and C- termini of α-helical segments. The 3_{10}-helix conformation is characterized by an i(CO) → i + 3(NH) hydrogen bond pattern, three residues per turn and backbone torsion angles attaining values close to $\Phi = \pm 49°$ and $\psi = \pm 26°$. Due to the achiral nature of Aib, left- and right-handed helices occur with the same probability. It was found that Aib-containing peptides with $n \leq 8$ preferentially attain a 3_{10}-helix conformation, while in longer peptides ($n \geq 10$) the α-helical structure predominates.[23] As a consequence, the peptides investigated in this contribution may be considered as helical building blocks ideally formed by two (n = 6, 3_{10}-helix), three (n = 12, α-helix), and four (n = 15, α-helix) turns (Figure 1).

The conformationally constrained character of Aib, determined by the *gem*-dimethyl substitution on the C^α atom, confers to its homopeptides excellent β-sheet breaker properties.[24] For this reason, Aib-containing peptides have been investigated as possible therapeutic compounds inhibiting the formation of amyloid fibrils.[25] In this work, we analyzed the role of hydrophobic effects on the aggregation process, and how the morphology of the resulting aggregates is affected by

dx.doi.org/10.1021/jp400009j | J. Phys. Chem. B 2013, 117, 5448−5459

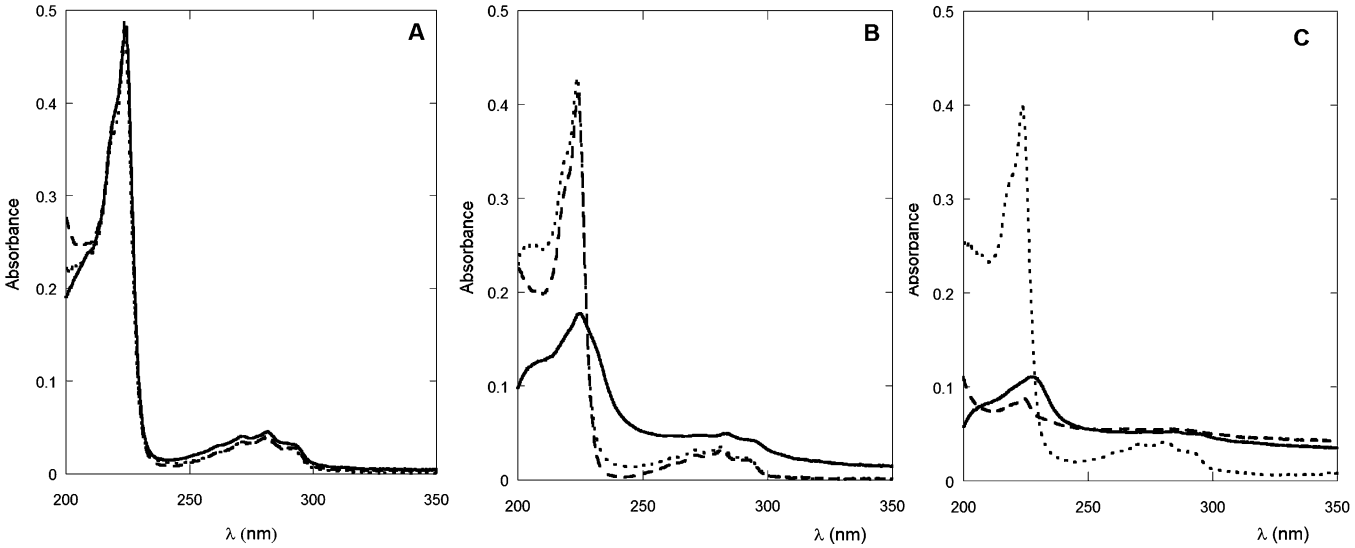

Figure 2. Absorption spectra of U_6N(A), $U_{12}N$ (B), and $U_{15}N$ (C) in methanol (dotted lines), $70/30_{(v/v)}$ methanol/water (long dashed lines), and $50/50_{(v/v)}$ methanol/water (full lines).

the increasing length of the helical peptides and the onset of specific aromatic−aromatic interactions.

These issues were tackled by investigating the aggregation propensity of the U_nN peptides in methanol/water (m/w) solutions of different composition by UV−vis absorption, fluorescence, and IR absorption spectroscopies and the morphology of peptide aggregates on a mica surface by atomic force microscopy (AFM) imaging.

MATERIALS AND METHODS

Materials. The synthesis and characterization of the peptides investigated in this work were already reported.[26] Acronyms are U_nN = Z-$(Aib)_nN$ (where Z = benzyloxycarbonyl; U, Aib = α-aminoisobutyric acid; N = −O−CH_2-CH_2−(1)naphthyl; n = 6, 12, 15). Only spectroscopy grade solvents (Carlo Erba, Milan, Italy) were used for all experiments. Low-conductive bidistilled water was used for the preparation of all of the m/w solutions.

Methods. *UV−vis Absorption.* Absorption measurements were carried out on a Cary 100 SCAN (Varian, Palo Alto, CA) spectrophotometer. Molar concentrations were determined in methanol by absorption measurements at λ = 280 nm [naphthyl absorption, $\varepsilon(280)$ = 6100 M^{-1} cm^{-1}]. All of the experiments were carried out in quartz cells of variable optical length (0.1, 0.5, and 1 cm) at micromolar concentrations.

Steady-State and Time-Resolved Fluorescence. Emission spectra of the investigated compounds at micromolar concentrations were obtained on a Spex-Fluorolog III (Horiba Jobin-Yvon Instruments, Middlesex, U.K.) spectrofluorimeter, equipped with a 450 W xenon lamp, and operating in single photon counting (SPC) mode. Samples were excited at 280 nm and the fluorescence spectra recorded from 300 to 500 nm using a bandwidth of 2 nm for both excitation and emission slits. Thioflavin (ThT) (Fluka, Büchs, Switzerland) assays[27] were carried out in $70/30_{(v/v)}$ m/w solutions at 10 μM peptide concentration and at a 2:1 ThT/peptide ratio. Samples loaded in a 1-cm quartz cuvette were excited at 440 nm, and the ThT fluorescence was recorded from 450 to 600 nm.

Fluorescence time decays were obtained by an EAI Life-Spec-ps (Edinburgh Analytical Instruments, Edinburgh, U.K.), operating in the SPC mode (λ_{exc} = 298 nm; λ_{em} = 340 and 400 nm; time interval = 500 ns; channels = 1024; excitation/emission bandwidths 8 nm). Excitation at λ = 298 nm was obtained by an IBH NanoLED light emitting diode (Horiba Jobin-Yvon Instruments, Middlesex, U.K.) with 1 ns nominal pulse duration. Experimental time decays were deconvoluted by the pulsed excitation profile through discrete multiexponential analysis by a standard software provided by EAI. Time distribution analysis of the experimental time decays was also performed without significant differences in the recovered time decay parameters. Concentration dependent time decay experiments on $U_{12}N$ were carried out in the concentration range from 20 to 320 μM. In this case, experimental decays were analyzed through a global fit with the constraint to reproduce all of the concentration dependent experiments with the same lifetimes, but with variable pre-exponential factors (amplitudes). For these experiments the excitation/emission bandwidths were fixed at 4 nm.

Fourier-Transformed Infrared (FTIR) Spectroscopy. FTIR spectra were recorded on a Nicolet FTIR spectrometer (Thermo Electron Co., Madison, WI) in the attenuated total reflection (ATR) mode on peptide films dried into a vacuum pump for 18 h on a ZnSe crystal. Spectra were recorded from 4000 to 700 cm^{-1} mediating over 256 scans with a resolution of 2 cm^{-1}.

Atomic Force Microscopy (AFM). AFM measurements on peptide films dried on a mica surface were performed in air using a Veeco Multiprobe IIIa (Santa Barbara, CA) instrument. Experiments were carried out at room temperature (20 °C) in the tapping mode by using NanoSensors SiO_2 tips with a force constant of about 40 N/m and a typical curvature radius on the tip of 7 nm. The contrast of the AFM images was enhanced for sake of clarity by using standard software supplied by Veeco Instruments. Force spectroscopy measurements were carried out operating in the contact mode by using Si_3N_4 tips with a spring constant of 0.48 N/m and an estimated curvature radius of 40 nm. Force plots were collected on the mica substrate close to the fibrils and were used to calibrate the deflection sensitivity of the instrument. Force/volume experiments were performed collecting 64 × 64 force plot arrays.[28]

Molecular Dynamics Calculations. Molecular dynamics (MD) simulations on U_6N and $U_{15}N$ in $70/30_{(v/v)}$ methanol/

dx.doi.org/10.1021/jp400009j | J. Phys. Chem. B 2013, 117, 5448−5459

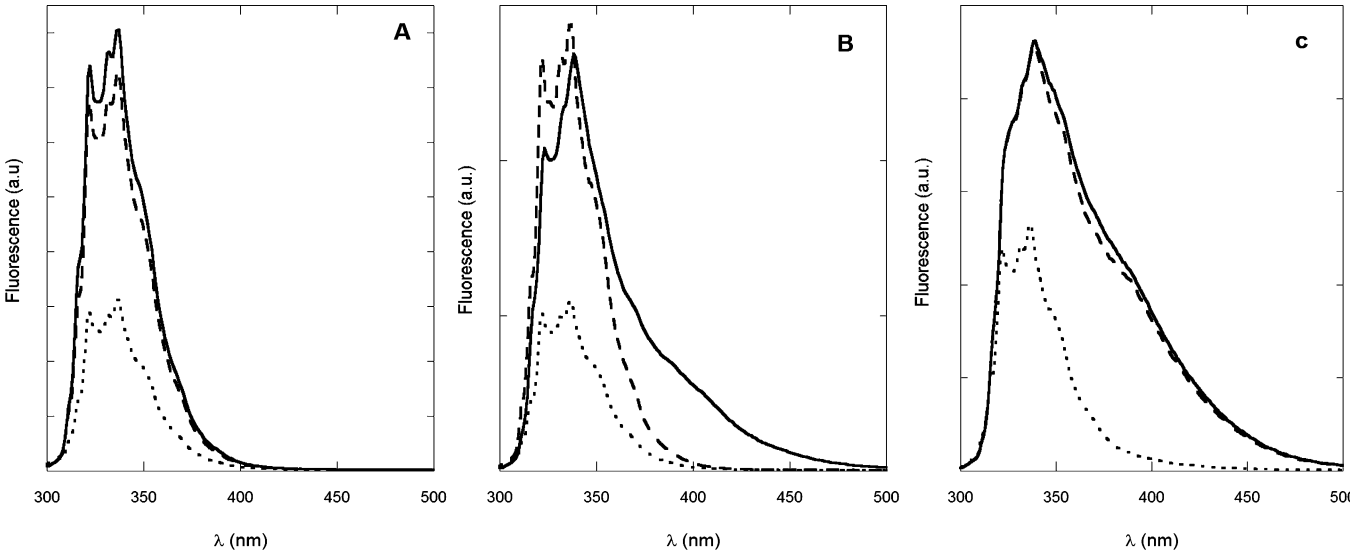

Figure 3. Fluorescence spectra of U_6N(A), $U_{12}N$ (B), and $U_{15}N$ (C) in methanol (dotted lines), $70/30_{(v/v)}$ methanol/water (long dashed lines), and $50/50_{(v/v)}$ methanol/water (full lines).

water solutions were carried out taking into account 6 peptide units initially disposed in 3_{10}- and α-helical conformations, respectively. Three different simulations were carried out considering 6 right-handed helical units, 6 left-handed helical units, and 3 right- and 3 left-handed helical units. MD simulations were carried out by using GROMACS 4.0.7,[29] with the ffG53a6 force field.[30]

RESULTS

UV−vis Absorption. The aggregation properties of U_nN (n = 6, 12, and 15) were investigated by UV−vis absorption spectroscopy in methanol, and $70/30_{(v/v)}$ and $50/50_{(v/v)}$ m/w solutions. As shown in Figure 2A, the UV−vis absorption spectrum of U_6N in methanol is dominated by the n → π^* [λ_{max} = 280 nm; $\varepsilon(280)$ = 6100 M^{-1} cm^{-1}] and $\pi \rightarrow \pi^*$ [λ_{max} = 220 nm; $\varepsilon(220)$ = 70 000 M^{-1} cm^{-1}] transitions of the naphthyl chromophore.[31] Amide transitions, occurring in the 190−240 nm region, are hidden by the predominant absorption of the aromatic groups. The absorption spectra of U_6N in $70/30_{(v/v)}$ and $50/50_{(v/v)}$ m/w solutions overlap the spectrum in methanol both in shape and intensity. Interestingly, no substantial changes of the UV−vis spectra of U_6N were observed in one-month aged methanol and m/w solutions. The lack of spectral perturbations was confirmed in the case of freshly prepared methanol and $70/30_{(v/v)}$ m/w solutions of $U_{12}N$ (Figure 2B). In contrast, the absorption spectrum of $U_{12}N$ in a $50/50_{(v/v)}$ m/w solution showed a lower intensity and a wide broadening of the transition at 225 nm. A slight red-shift of the absorption maximum and the appearance of a shoulder at lower wavelengths suggest formation of both H- and J-type aggregates. The occurrence of both types of aggregates has already been described in the literature, as a result of the combined effect of aromatic stacking interactions and hydrophobic effects driving the aggregation process.[32] A significant contribution of scattered light to the absorption spectrum of $U_{12}N$ in a $50/50_{(v/v)}$ m/w solution can be also observed, which suggests the presence of large aggregates in solution. In the case of $U_{15}N$, although the absorption spectrum in methanol maintains the typical absorption features of the naphthalene monomer, a strong decrease in intensity, together with a marked broadening of the $\pi \rightarrow \pi^*$ transition, can be observed in both freshly prepared $70/30_{(v/v)}$ and $50/50_{(v/v)}$ m/w solutions (Figure 2C). The latter absorption spectra are markedly red-shifted and heavily affected by diffuse light contamination, the weak n → π^* transition being hardly detectable. However, it should be emphasized that no significant variations in the absorption features of both $U_{12}N$ and $U_{15}N$ peptides could be detected after one month for all the solutions investigated. This finding indicates that the aggregated species are stable even in solutions characterized by a high content of water.

Steady-State Fluorescence. Further evidence on the formation of aggregated species for the longer homologues of the U_nN peptide series was provided by steady-state fluorescence measurements (Figure 3). Much like the absorption spectra, the emission spectra of U_6N in methanol, $70/30_{(v/v)}$ and $50/50_{(v/v)}$ m/w solutions are typical of the unperturbed naphthyl fluorophore, showing well-resolved vibronic transitions between 310 and 370 nm (Figure 3A). Stronger fluorescence intensities have been obtained in m/w solutions with respect to pure methanol, due to the lower efficiency of oxygen quenching in aqueous solutions. Confirming the UV−vis absorption results, also the emission spectral features of U_6N did not significantly change in one-month aged methanol and m/w solutions. The emission spectra of $U_{12}N$ in methanol, and $70/30_{(v/v)}$ and $50/50_{(v/v)}$ m/w solutions revealed a peculiar trend that parallel the results of UV−vis absorption (Figure 3B). Indeed, while the fluorescence spectra in methanol and $70/30_{(v/v)}$ m/w solutions are typical of the naphthyl monomer emission, the latter being remarkably more intense because of the less efficient oxygen quenching, the emission spectrum in a $50/50_{(v/v)}$ m/w solution is characterized by loss of the vibronic structure and the onset of a broad, red-shifted emission typical of naphthalene excimers.[33] Excitation spectra measured at λ_{em} = 340 and 400 nm in $70/30_{(v/v)}$ m/w (data not shown) overlap the absorption spectrum of $U_{12}N$, which highlights the excited state character of the interaction leading to the formation of excimer species.

Emission spectra of methanol aged solutions of $U_{12}N$ are stable at all times, while those measured for $70/30_{(v/v)}$ m/w

dx.doi.org/10.1021/jp400009j | J. Phys. Chem. B 2013, 117, 5448−5459

Table 1. Relative Quantum Yields of the Peptides in Methanol and m/w Solutions at Different Times

	quantum yields at t = 0			after a week			after one month		
solution	U_6N	$U_{12}N$	$U_{15}N$	U_6N	$U_{12}N$	$U_{15}N$	U_6N	$U_{12}N$	$U_{15}N$
methanol	1	0.93	0.96	0.97	0.94	0.99	0.97	0.99	1.4
70/30 m/w	1	0.97	4.5	0.97	0.91	4.4	1.02	1.2	4.6
50/50 m/w	1	1.8	4.0	1.02	2.3	4.1	1.01	2.7	4.6

solutions slowly evolved toward the spectral features observed in the case of freshly prepared $50/50_{(v/v)}$ m/w solutions. The fluorescence spectra of $U_{15}N$ in methanol, and $70/30_{(v/v)}$ and $50/50_{(v/v)}$ m/w solutions (Figure 3C) featured the typical emission of the naphthyl monomer in methanol, but in both $70/30_{(v/v)}$ and $50/50_{(v/v)}$ m/w solutions the loss of vibronic structure and a very strong red-shifted emission indicate the formation of excimer species and/or highly fluorescent J-type aggregates. Also in this case, the excitation spectra, taken at λ_{em} = 340 and 400 nm, were found to overlap the absorption spectrum, suggesting that the naphthyl groups are separated by more than 3−4 Å, the typical distance for the onset of short-range aromatic−aromatic interactions. It should be noted that the emission spectra of aged (one month) m/w solutions of $U_{15}N$ did not reveal significant changes, which highlights the stability of aggregated species in solution.

To summarize the results of steady-state fluorescence experiments, the quantum yields of the three peptide homologues in methanol and m/w solutions investigated at different times are reported in Table 1. Data at all times are normalized to the emission intensities of U_6N a t = 0 (fresh solutions) in the different environments, i.e., methanol, $70/30_{(v/v)}$ m/w, and $50/50_{(v/v)}$ m/w, respectively.

It can be noted that in methanol all samples are stable as monomers at all times (only for one-month aged solutions of $U_{15}N$ a slight increase in the fluorescence intensity could be detected). However, although U_6N did not show any propensity to aggregate in all of the m/w solutions investigated, $U_{15}N$ formed highly fluorescent species in both $70/30_{(v/v)}$ and $50/50_{(v/v)}$ m/w solutions, characterized by a strong excimer-like emission.

Interestingly, $U_{12}N$ showed an intermediate behavior, being rather stable as a monomer in $70/30_{(v/v)}$ m/w and giving rise to a slow aggregation process in a $50/50_{(v/v)}$ m/w solution. These findings clearly emphasize the importance of hydrophobic interactions in solutions with a high content of water but also highlight the role of the stabilization of the helical structure with elongation of the peptide chain in driving the aggregation process.

Interesting results were obtained when the ThT assay was applied to $70/30_{(v/v)}$ m/w solutions of U_6N, $U_{12}N$, and $U_{15}N$ (Figure 4). ThT is well-known to bind selectively to peptide β-sheet structures, showing a substantial increase of its fluorescence quantum yield.[34] For this reason, ThT has been extensively used as a marker in the diagnostics of amyloid fibrils. As can be seen from Figure 4, ThT exhibited similar emission intensities not only with U_6N and $U_{12}N$, as expected from the UV−vis absorption and steady-state fluorescence data reported above, but also in the case of $U_{15}N$ that was shown to aggregate in this environment. These results strongly support the view that $U_{15}N$ aggregates are formed by self-assembled helical chains.

Time-Resolved Fluorescence. Time-resolved fluorescence measurements in methanol and in $70/30_{(v/v)}$ and $50/50_{(v/v)}$ m/w solutions were carried out to further analyze the aggregation

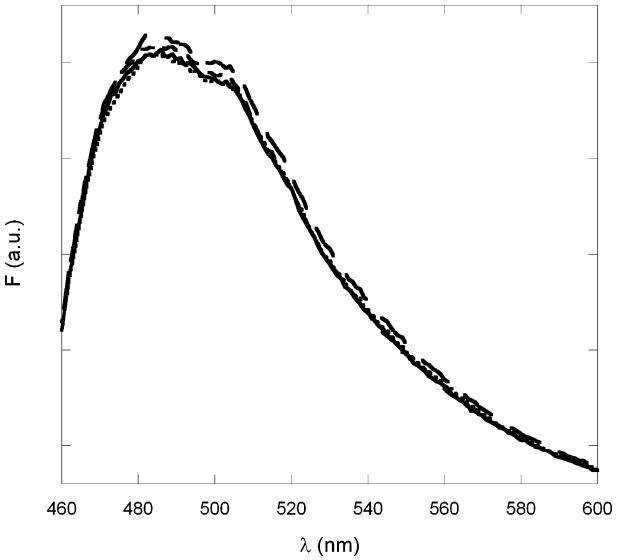

Figure 4. ThT emission in 70/30(v/v) methanol/water solution of ThT (full line) and ThT with U_6N (dotted line), $U_{12}N$ (dashed line), and $U_{15}N$ (long dashed line). Peptide concentration: 10 μM.

properties in solution of the peptides investigated. The experiments were carried out at λ_{em} = 340 and 400 nm to discriminate between the emission features of monomer and excimer and/or J-aggregate species, respectively. The associated time-decay parameters were obtained by fitting the experimental results by a discrete multiexponential function, i.e.

$$I(t) = \sum_i \alpha_i e^{-t/\tau_i} \quad (1)$$

The values are reported in Tables 2 (λ_{exc} = 298 and 340 nm) and 3 (λ_{exc} = 298 and 400 nm). In all cases, the emission decay of U_6N can be described by a single lifetime, which in view of

Table 2. Fluorescence Time Decay Parameters for (a) the Peptides in Methanol, (b) the Peptides in $70/30_{(v/v)}$ m/w, and (c) the Peptides in $50/50_{(v/v)}$ m/w (in All Cases: λ_{exc} = 298 nm; λ_{em} = 340 nm)

	τ_1 (ns)	α_1	τ_2 (ns)	α_2	$\langle\tau\rangle$ (ns)	χ^2
			(a)			
U_6N	15.6	1				1.16
$U_{12}N$	15.9	1				1.03
$U_{15}N$	15.4	0.96	41.4	0.04	16.4	1.05
			(b)			
U_6N	35.5	1				1.15
$U_{12}N$	28.1	0.46	46.9	0.54	38.2	1.10
$U_{15}N$	20.9	0.49	57.5	0.51	39.6	1.31
			(c)			
U_6N	40.6	1				1.15
$U_{12}N$	23.8	0.23	52.8	0.77	46.1	1.10
$U_{15}N$	22.9	0.51	54.9	0.49	38.6	1.31

dx.doi.org/10.1021/jp400009j | J. Phys. Chem. B 2013, 117, 5448−5459

Table 3. Time Decay Parameters for the Peptides in 50/50$_{(v/v)}$ m/w λ_{exc} = 298 and 400 nm (λ_{exc} = 298 nm; λ_{em} = 340 nm)

	τ_1	α_1	τ_2	α_2	τ_3	α_3	χ^2
$U_{12}N$	50.8	0.72	84.5	0.27			1.23
$U_{15}N$[a]	3.5	−0.17	61.0	0.46	87.5	0.24	1.21
$U_{15}N$	3.7	−0.24	52.9	0.34	81.7	0.40	1.13

[a]In 70/30$_{(v/v)}$ m/w.

the spectral evidence discussed above, was assigned to the naphthyl monomer emission in that specific environment. The longer lifetimes measured for U_6N in water-rich solutions parallel the increasing emission quantum yields measured by steady-state experiments, due to less efficient oxygen quenching. Radiative rate constants can be obtained from the measured quantum yields and time decays, i.e., $k_r = \Phi/\tau$. For U_6N, we obtained $k_r = 1.4(\pm 0.1) \times 10^8$ s^{-1} in all of the solutions investigated. The time decays of $U_{12}N$ and $U_{15}N$ in methanol are predominantly accounted for by monomer-like emission. A second time decay component, characterized by a small pre-exponential factor and a long lifetime, was also detected for $U_{15}N$ in methanol. The contribution of this long time decay becomes more and more important with increasing the fraction of water in the solvent mixtures and it accounts for around 70% of the fluorescence intensity for $U_{12}N$ and $U_{15}N$ in 70/30$_{(v/v)}$ and 50/50$_{(v/v)}$ m/w solutions. To better characterize the species, excimers and/or fluorescent J-type aggregates, associated to the slow time decay component (red-shifted emission), we carried out time-resolved experiments at λ_{em} = 400 nm in 50/50$_{(v/v)}$ m/w solutions for $U_{12}N$ and $U_{15}N$ (the U_6N emission at 400 nm can be hardly detected). From the data reported in Table 3, it can be noted that the time decays at λ_{em} = 400 nm of both $U_{12}N$ and $U_{15}N$ are characterized by two very long time components, the faster clustering around 50−60 ns and the slower around 85 ns. The faster component is similar to the long lifetime measured at λ_{em} = 340 nm (excimer emission), whereas the slower component can be tentatively ascribed to the fluorescence of J-type aggregates.[20] Interestingly, the time decay of $U_{15}N$ reveals a short lifetime characterized by a negative amplitude, indicative of the onset of the excited state process leading to excimer formation.

Multicomponent time decays have been observed in the case of pyrene excimers in organized media or organic polymeric glasses, where a short lifetime (∼5 ns) was attributed to the blue-shifted emission of an excited ground state dimer, while a slower time decay (∼35 ns) was ascribed to the red-shifted excimer observed in steady-state spectrum.[35] This finding reflects a continuum of aromatic−aromatic interactions, involving the formation of both ground and excited state complexes, characterized by a distribution of distances and orientations and classified for simplicity in the two "extreme" topological classes of H- or J-type aggregates (ground state complexes, sometimes referred as "static excimers") and excimers (pure excited state complexes, "dynamic excimers").[35] Formation of dynamic excimers requires a diffusive encounter between the naphthyl units and the excitation localized on one of them. They are characterized by excitation spectra that strictly overlap the absorption spectra and, in a time-resolved experiment, by a negative component associated to the growth of the excimer emission. The excimer state has been described by a mixing of exciton and charge-separated resonance states, both favored by a sandwiched conformation of the interacting aromatic units. In static excimers, the aromatic units are so close that they exhibit perturbed absorption and excitation spectra. The ground-state surface shows a minimum at a separation distance intermediate between that of electronically isolated molecules (monomer emission) and the onset of π-orbital repulsion (∼3 Å), whereas the excited-state surface exhibits a double minimum and wavelength-dependent multicomponent time-decays. In our experiments, we obtained perturbed absorption spectra, overlapping excitation/absorption spectra, intense and structureless red-shifted emissions and complex time-decays, which suggests that, in our samples, the naphthyl units attain a continuum of separation distances and different orientations, giving rise to a manifold of intermolecular conformations leading to nonfluorescent (H-type), highly fluorescent ground-state (J-type or "static excimers"), and pure excited state ("dynamic excimers") species.

Time-resolved fluorescence experiments were also carried out in a 70/30$_{(v/v)}$ m/w solution varying the peptide concentration from 0.25 μM to 500 μM (λ_{em} = 340 nm). The experimental time decays were analyzed by a global fit, i.e., a linked procedure that constrains all experimental data to be fit by the same lifetimes, but allows the pre-exponential factors to vary without restrictions. Limiting the number of lifetime components to two, as suggested by the already reported time-resolved experiments, implies that we cannot distinguish among aggregates formed by a different number (n) of peptide units or between excited state (excimer) or fluorescent ground-state complexes (J-type aggregates). It results that the U_6N time decays can be described by a single lifetime (35 ± 2 ns), indicating that U_6N is present as a monomer species in the entire concentration range investigated. In the case of $U_{15}N$, the experimental decays can be well reproduced by two lifetimes with the same pre-exponential factors of 0.5 at all concentrations. This finding indicates that the aggregation process of $U_{15}N$ in 70/30$_{(v/v)}$ m/w solution is already completed at 0.25 μM and that the attained equilibrium is stably conserved up to the maximum concentration investigated (500 μM). The trend observed for $U_{12}N$ is more complex, and its analysis gives important insights on the aggregation process. Actually, the global analysis of the $U_{12}N$ time decays afforded two lifetimes, the shorter centered at 34 (±2) ns, typical of monomer emission, and the longer at 53 ns, characteristic of excimers or weakly bound aggregated species. In Figure 5 the variation of the pre-exponential factors (amplitudes) obtained

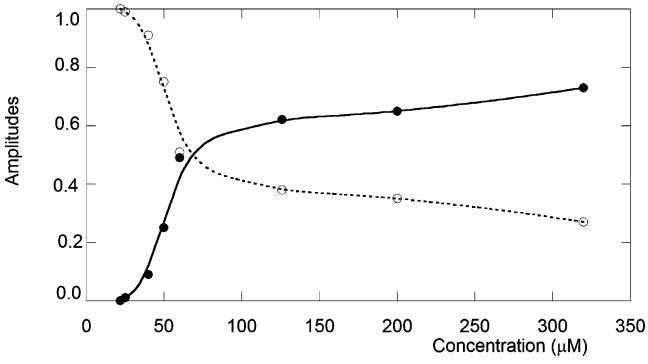

Figure 5. Amplitudes (pre-exponential factors) as provided by global fit of $U_{12}N$ time decays in 70/30$_{(v/v)}$ m/w solution at variable peptide concentration (micromolar). Empty circles, α_1(monomer); filled circles, α_2(excimers or weakly bound aggregates).

dx.doi.org/10.1021/jp400009j | J. Phys. Chem. B 2013, 117, 5448−5459

by the global fit of the experimental time decays of $U_{12}N$ in 70/30$_{(v/v)}$ m/w solution at different peptide concentrations is reported.

Between 20 and 60 μM peptide concentration, a rapid decrease of the monomer component can be observed, followed by a slow asymptotic decrease at higher peptide concentrations. Significantly, at low concentrations, the amplitude versus concentration trend shows a marked sigmoid character, typical of a cooperative aggregation process.

Assuming the single equilibrium $n\mathrm{M} \rightleftarrows \mathrm{M}_n$ and introducing the associated aggregation constant in terms of the monomer (x_m) and aggregate (x_a) molar fractions, one obtains[36]

$$K_A^{n-1} = \frac{x_a}{x_m^n} \quad (2)$$

The amplitudes α_2 can be directly related to f_a, i.e., the number fraction of peptide aggregates:

$$f_a = \frac{nx_a}{x_p} \quad (3)$$

where $x_p = x_m + nx_a$. Combining eqs 2 and 3, the dependence of the fraction of aggregates on the total peptide fraction (x_p) can be obtained:

$$\frac{f_a}{(1-f_a)^n} = n(K_A x_p)^{n-1} \quad (4)$$

The experimental amplitudes α_2 (=f_a) were fitted by eq 4, providing a value for the association constant $K_A = 7(\pm 1) \times 10^5$ and the number (n) of monomers forming the aggregate M_n (Supporting Information). Unfortunately, the fitting function of eq 4 is not very sensitive to the parameter n, and, as a result, values of n between 14 and 100 give a comparable satisfactory fit of the experimental data.

These results indicate that the interaction between the naphthyl chromophores in the different environments, i.e., from methanol to 50/50$_{(v/v)}$ m/w, is modulated by the extent of hydrophobic effects that lead the two aromatic units to collapse to a short distance (3−4 Å). The evolution of the fluorescence spectra from an excimer-like emission, characteristic of relatively long distances between the naphthyl units, to a J-type emission, characteristic of the formation of weakly bound fluorescent ground state complex, as also shown by the absorption spectra in the different environments, is ruled by the onset of short-range $\pi-\pi$ interactions between the aromatic moieties, the organization of the solvent molecules in the proximity of aromatic surfaces, and the increasing bulk dielectric constant with increasing water content of the m/w solvent mixtures.[37] However, the experiments reported here show that, in the explored concentration range, the hydrophobic effect is not the only factor determining the aggregation properties of the peptides investigated. Analyzing the fluorescence results along the Aib homopeptide series from n = 6 to 15, it appears that the dynamical and structural properties of the peptide backbone, and in particular the stabilization of the helical conformation with the elongation of the peptide chain (and hence the onset of interhelical interactions), are the effective driving forces of the aggregation process.

Fourier-Transformed Infrared Spectroscopy (ATR-FTIR). Fourier-transformed infrared (FTIR) measurements in the attenuated total reflectance (ATR) mode on dried peptide films were carried out to obtain information on the peptide secondary structures. In Table 4 the frequencies of the most intense IR absorption bands are reported for all peptides investigated.

Table 4. Infrared Absorption Wavenumbers (cm^{-1}) for Dried Films of the U_nN Peptides

U_6N (10 μM)	3330, 3458	1653	1534	1460	1240
$U_{12}N$ (10 μM)	3298	1665, 1658	1581, 1537		
$U_{12}N$ (125 μM)	3309	1656	1535	1457	1383
$U_{15}N$ (10 μM)	3289	1665, 1658	1547, 1534	1468	

The experimental wavenumbers are found to cluster in the regions around 3300 cm^{-1} (amide A, N−H stretching), 1660 cm^{-1} (amide I), and 1540 cm^{-1} (amide II).[38] As for the N−H stretching frequencies, all peptides exhibit an intense band centered at 3300 cm^{-1}, typical of H-bonded N−H groups.[39] Only U_6N shows a significant absorption at 3458 cm^{-1}, which indicates that, even in the U_6N dried film, a significant fraction of the peptide NH groups is not involved in any H-bonding interaction. All peptides feature strong absorption bands in the carbonyl stretching (amide I) region around 1660 cm^{-1}, characteristic of helical structures. The position of the amide II transition also suggests the onset of helical conformations. Additional peaks at 1460 and 1260 cm^{-1} are assigned to the bending of the methyl groups of the Aib units and to the amide III transition.[38] In agreement with the results provided by the ThT assay, no experimental frequencies ascribable to β-sheet like structures could be detected.

Atomic Force Microscopy (AFM). AFM measurements were carried out on dried peptide films obtained by a 24-h deposition of m/w solutions of variable composition and concentration on mica surfaces. A typical AFM image of U_6N on mica deposited from a 10 μM 70/30$_{(v/v)}$ m/w solution is shown in Figure 6. Globular structures characteristics of nonspecific aggregation driven by hydrophobic effect are predominantly observed, as it is generally found in the case of nonspecific aggregation of apolar molecules.[40] Small filaments of 200 nm maximum length were also rarely observed in limited regions of the sample.

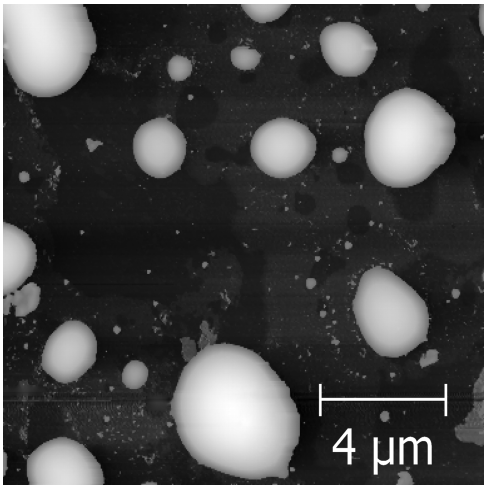

Figure 6. AFM image of U_6N on mica. Deposition solution: U_6N 10 μM in 70/30$_{(v/v)}$ m/w solution.

In the case of $U_{12}N$, deposited under the same experimental conditions, globular structures and fibrils were observed in

dx.doi.org/10.1021/jp400009j | J. Phys. Chem. B 2013, 117, 5448−5459

comparable amounts. The latter appear to be longer (500 ± 100 nm, width 40 ± 10 nm) with respect to the similar structures rarely observed in the case of U_6N. On the other hand, micrometric filaments (with width of 100 ± 10 nm) were predominantly found for $U_{15}N$ deposited from a 10 μM 70/30$_{(v/v)}$ m/w solution (Figure 7).

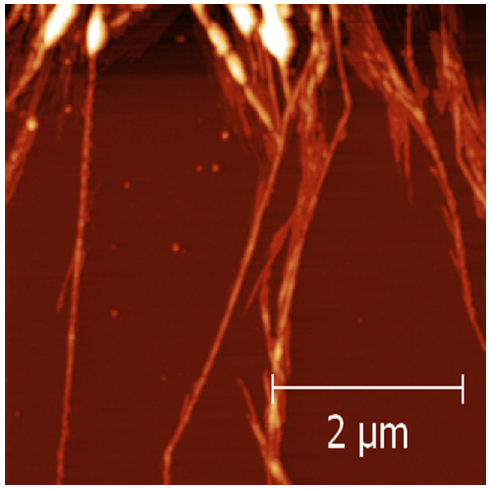

Figure 7. AFM image of $U_{15}N$ on mica. Deposition solution: $U_{15}N$ 10 μM in 70/30$_{(v/v)}$ m/w solution.

Interesting results were obtained for $U_{12}N$ films dried on mica from a $U_{12}N$ 125 μM 70/30$_{(v/v)}$ m/w solution. In this case, very long fibril structures (2−10 μm) were predominantly observed (Figure 8), which show an internal helical arrangement (helix rise: 360 ± 70 nm). It should be noted that both left- and right-handed fibrils are spotted in the AFM image (Figure 8, left). This effect nicely reflects the achiral nature of the Aib homopeptide building blocks, making left- and right-handed helices energetically equivalent.

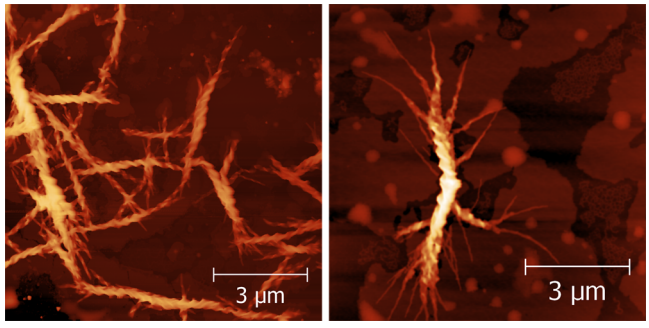

Figure 8. AFM images of $U_{12}N$ on mica. Deposition solution: $U_{12}N$ 125 μM in 70/30$_{(v/v)}$ m/w solution.

This finding supports the view that the secondary structure attained by the single peptide chain may tune the morphology of the mesoscopic aggregates. Preliminary molecular dynamics (MD) simulations, carried out on U_6N and $U_{15}N$ in 70/30$_{(v/v)}$ m/w solution, revealed that only the longer peptide is able to form stable and ordered arrays of helical peptide layers (Figure 9A). Most interestingly, densely packed multilayers were obtained only when left-handed and right-handed helical layers self-assemble in an alternate order. Simulations carried out with only left-handed or right-handed peptide helices did not give rise to stable peptide aggregates. This finding clearly highlights the peculiar aggregation properties of Aib-based peptides, and gives an important clue on the β-sheet breaking properties of C^{α}-tetrasubstituted achiral peptides. This point clearly deserves a more extensive investigation that we prefer to report in the next future. A sketch of the aggregation mechanism leading from the single peptide helix to the mesoscopic fibril, imaged by AFM experiments, is reported in Figure 9B.

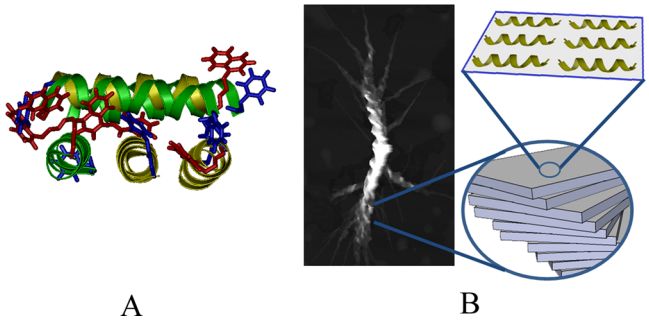

Figure 9. (A) Peptide aggregate resulting from MD simulation of left- and right-handed $U_{15}N$ peptide units. (B) Schematic draft of the aggregation process leading to the observed helically arranged peptide fibrils.

Interesting information is obtained when we applied AFM force spectroscopy in order to characterize the internal packing of the peptide fibrils. If the cantilever and a fiber can be considered as two serial oscillators, then the fibril spring constant (k_s) is

$$k_s = (k_{tip}k_{tot})/(k_{tip} - k_{tot}) \quad (6)$$

Measurements on four different fibrils provided the spring constant values k_s = 2.8(±0.3), 3.4(±0.6), 5.3(±0.8), and 7.2(±0.7) N/m, respectively, indicating some heterogeneity of the fibrils. The associated Young's modulus can be obtained from the Hertzian model[41]

$$F^{2/3} = C - \left[\frac{4E\sqrt{R}}{3(1-\sigma^2)}\right]^{2/3}\Delta \quad (7)$$

Where Δ is the sample-to-tip distance, F the load, R the tip radius of curvature, and σ the Poisson ratio, an elastic parameter characteristic of the material (for a fibril material σ = 0.3 is tipically assumed). Finally, we obtained the Young's modulus for the four fibrils investigated, i.e., G = 6.6(±0.6), 6.7(±0.6), 11(±1), and 15(±1) MPa, respectively. These values are almost 2 orders of magnitude smaller than those typical of crystals of globular proteins (20−1 GPa), and at least 1 order of magnitude smaller than those obtained in the case of amyloid fibrils (4−0.6 GPa).[42−45] This finding supports the idea that the aggregates formed by the helical peptides here investigated are stabilized by weak aromatic interactions and hydrophobic effect, giving rise to "softer" mesoscopic structures.

DISCUSSION

Amyloids are normally soluble, and any excess is generally cleared away. When these peptides become insoluble, however, they associate in the space between cells forming amyloid fibrils, the aggregation process being accompanied by a structural transition from the native folding status to a predominant β-sheet secondary structure.[46] Then, the resulting large senile plaques (SP) damage the brain cells and attract

dx.doi.org/10.1021/jp400009j | J. Phys. Chem. B 2013, 117, 5448−5459

reactive cells, microglia and astrocytes, which cause further deterioration.

SP fibrils have been therefore believed to be involved in neurotoxicity. However, in the Alzheimer's disease, experimental evidence has been accumulated indicating that in the initial phase of fibril formation, soluble peptide oligomeric precursors, formed by 40- to 42-residue peptides (Aβs), might be the toxic species, rather than mature fibrils.[47] Extensive X-ray diffraction and electron microscopy studies demonstrated that Aβs form characteristic β-sheet rich fibrils, 6−8 nm in diameter, in which the direction of the peptide chains is perpendicular to the fibril long axis.[48] Fibrillization appears to occur via a prefibrillar stage consisting of small spherical multimers that are consumed as fibrillization proceeds. The species isolated at the early stages of aggregation were characterized as protofibrillar aggregates, 20−70 nm in length and ∼3 nm in diameter, suggesting a nucleation dependent mechanism.[13,49]

AFM studies on Aβs deposited on hydrophilic mica exhibited a pronounced dependence on the peptide concentration: at low concentration Aβs formed pseudomicellar aggregates, while at higher concentration Aβs showed the tendency to produce linear assemblies, reminiscent of protofibrillar assemblies.[40]

These findings clearly parallel the AFM results reported above with varying U_nN peptide length and concentration. In the present study, we tuned the hydrophobic conditions which trigger peptide aggregation by adding increasing fraction of water to methanol solutions.

The peptide systems investigated here focus on two main aspects of the peptide aggregation process: (i) The effect of aromatic moieties. We faced this point by functionalizing the peptide chain with a naphthyl group in addition to the N-terminal benzyl group. (ii) The secondary structure attained by the peptide main chain. This issue was investigated by studying helical oligopeptides exclusively formed by C^{α}-tetrasubstitued amino acids.

The specific effect of aromatic moieties in driving the aggregation of amyloids has been extensively investigated, focusing in particular on the FF motif of the Aβ segments, thought to be the key element which promotes the formation of the β-sheet aggregates.[50] FF dipeptides have been shown to aggregate in different nano- and mesoscopic structures (nanotubes, nanodisks, and hydrogels) depending on the experimental conditions.[50,51]

However, further investigations suggest that aromatic−aromatic interactions might contribute to, but not be essential for, the stabilization of the aggregates, and that hydrophobicity, more than aromaticity, may be the driving force for assembly.[37] Other evidence indicates that aromatic−aromatic interactions are not required for amyloid fibril formation, but do influence the rate of fibril formation and the final fibril morphology.[52]

Our results support the view that the naphthyl group not only promotes peptide aggregation by enhancing the hydrophobic effect, but that the regular spatial organization of the naphthyl aromatic groups leading to formation of excimers and J-type aggregates contributes to the directional growth of the peptide fibrils, as recently found by Adams and co-workers.[53] That the specific pattern of aromatic stacking could influence the morphology of the nano- and mesoscopic aggregates has been already suggested in earlier studies on amyloid aggregation.[50] This finding has been associated to a stepwise mechanism of amyloid formation, the first step being characterized by nucleation of small aggregates, the geometry of which is determined by restricted $\pi-\pi$ stacking. The stepwise addition of further monomers propagates the same arrangement on a larger scale.

However, our results show that aromatic−aromatic interactions are not the only actors in this process and do not determine by themselves the pathway leading to fibril formation. In our case, this mechanism is undoubtedly promoted by the elongation of the helical peptide chain along the series U_6N, $U_{12}N$, and $U_{15}N$, as revealed by our spectroscopic experiments in solution, AFM imaging and preliminary MD results. Therefore, the transition from globular to fibril-like structures should be considered as governed by the ordered wrapping of helical peptide segments of sufficient length, i.e., 3−4 helix turns like those attained by $U_{12}N$ and $U_{15}N$, stabilized by aromatic−aromatic interactions.

In a seminal paper, Aggeli et al.[54] showed that peptides may form a variety of structural morphologies of increasing complexity, from tapes to ribbons (double tapes), fibers (stacked tapes), and fibrils (entwined fibers). This hierarchical self-assembly was proved to stem from the chirality of the individual peptide elements. β-Sheet ribbons have an intrinsically left-handed twist, because of the L-chirality of the peptide building blocks. On a larger scale, fibrils show a well-defined screw-like structure, with a finite width that is determined by the inherent chirality of the amino acid units and the elastic cost of bending, and adjust their twist in response to packing constraints. Consequently, helical ordering is observed within the fibrils, as a result of the preferred left-handed twist of the antiparallel β-sheets.[8,55]

In our case, the observed fibril-like structure maintains the memory of the rigid helical organization of the conformationally constrained peptide building blocks, inhibiting the formation of extended β-sheet structures, as proved by our IR absorption measurements and the ThT assay. Furthermore, the achiral nature of the poly$(Aib)_n$ chain makes right- and left-handed helices equally probable, which in turn determines the random twisting of the peptide fibrils observed in our AFM experiments. Preliminary MD results suggest that the presence of both right- and left-handed helices is necessary for the formation of densely packed peptide layers, from which helically arranged mesoscopic structures can be nucleated.

What it is most important from the point of view of potential therapeutic applications of the peptides investigated, fluorescence studies on one-month aged solutions demonstrated that peptide aggregates are relatively stable and do not tend to coalesce further or to precipitate.

On the basis of the experimental evidence which shows that partial denaturation of a few proteins leads to fibrillization and that proteins lacking specific secondary structure can fibrillize, the question of whether amyloid fibrillization results from partially folded intermediates has recently been addressed.[8] In the peptides investigated in this work, the rigidity of the helical structure attained by the poly$(Aib)_n$ backbone inhibits the formation of the β-sheet structures required in the first fibril self-assembly steps.

This finding has already inspired the possibility to use Aib-based peptides as therapeutic agents in Alzheimer or associated diseases.[25] It was suggested that an inhibitor that contains an aromatic recognition element together with a fibril breaker could bind to oligomers potentially evolving in amyloid structures, thus inhibiting the formation of larger aggregates.[50] The naphthyl-substituted Aib homopeptides discussed in this study appear to be promising lead compounds to achieve this goal.

dx.doi.org/10.1021/jp400009j | J. Phys. Chem. B 2013, 117, 5448−5459

CONCLUSIONS

The aggregation properties of model helical oligopeptides were investigated by optical spectroscopy (mainly steady-state and time-resolved fluorescence) and AFM imaging. The aggregation process was triggered by the hydrophobic effect exerted by increasing the water fraction in m/w solutions.

Peptide aggregation is enhanced by functionalization of the peptide chain with a naphthyl chromophore, but the formation of fibril-like structures is obtained only when the peptide chain forms a sufficiently long helix. The stability of the secondary structure for such short peptides is achieved due to the unique properties of the Aib residues that severely restrict the allowed conformational space.[5,22]

Both thioflavine assay and FTIR absorption experiments indicate that even mature peptide aggregates do not attain the toxic β-sheet conformation, while AFM imaging of peptide aggregates on a hydrophilic mica substrate reveals that the originally imprinted helical organization is propagated to the mesoscopic scale. These findings confirm the great interest for potential applications of conformationally constrained peptides as β-sheet breaker agents in the therapy of Alzheimer and related diseases.[24,25]

ASSOCIATED CONTENT

Supporting Information

1. Fitting of the amplitudes (pre-exponential factors) provided by experimental time decays at different concentrations of $U_{12}N$ in $70/30_{(v/v)}$ m/w solution by eq 4. 2. Size distribution of U_6N aggregates reported as the radius of equivalent ellipsoid mimicking the globular aggregates. This material is available free of charge via the Internet at http://pubs.acs.org.

AUTHOR INFORMATION

Corresponding Author

*E-mail: venanzi@uniroma2.it.

Notes

The authors declare no competing financial interest.

ACKNOWLEDGMENTS

This work was supported by the Italian Minister of University and Research (MIUR), PRIN 2010-2011 No. 2010FM738P – Photophysical and photochemical properties of organic and biological compounds in solution and in organized systems.

REFERENCES

(1) (a) Hartgerink, J. D.; Beniash, E.; Stupp, S. I. Self-Assembly and Mineralization of Peptide-Amphiphile Nanofibers. *Science* **2001**, *294*, 1684–1688. (b) Hartgerink, J. D.; Beniash, E.; Stupp, S. I. Peptide-Amphiphile Nanofibers: A Versatile Scaffold for the Preparation of Self-Assembly Materials. *Proc. Natl. Acad. Sci. U.S.A.* **2002**, *99*, 5133–5138. (c) Bianco, A.; Venanzi, M.; Aleman, C. Special Issue on Peptide-based Materials: from Nanostructures to Applications (Editorial). *J. Pept. Sci.* **2011**, *17*, 73–74.

(2) Looger, L. L.; Dwyer, M. A.; Smith, J. J.; Hellinga, H. W. Computational Design of Receptor and Sensor Proteins with Novel Functions. *Nature* **2003**, *423*, 185–190.

(3) Yasutomi, S.; Morita, T.; Imanishi, Y.; Kimura, S. A Molecular Photodiode System that Can Switch Photocurrent Direction. *Science* **2004**, *304*, 1944–1947.

(4) Zhang, S.; Marini, D. M.; Hwang, W.; Santoso, S. Design of Nanostructured Biological Materials through Self-Assembly of Peptides and Proteins. *Curr. Opin. Chem. Biol.* **2002**, *6*, 865–871.

(5) (a) Venkatraman, J.; Venkatraman, S. C.; Balaram, P. Design of Folded Peptides. *Chem. Rev.* **2001**, *101*, 3131–3152. (b) Toniolo, C.; Crisma, M.; Formaggio, F.; Peggion, C. Control of Peptide Conformation by the Thorpe-Ingold Effect (C^{α}-Tetrasubstitution). *Biopolymers (Pept. Sci.)* **2001**, *60*, 396–419. (c) Formaggio, F.; Broxterman, Q. B.; Toniolo, C. Synthesis of Peptides and Peptidomimetics. *Houben-Weyl Methods of Organic Chemistry*; Goodman, M., Felix, A., Moroder, L., Toniolo, C., Eds.; Thieme: Stuttgart, Germany, 2003; Vol. *E22c*, pp 292–310.

(6) (a) Whitesides, G. M.; Mathias, J. P.; Set, C. T. Molecular Self-Assembly and Nanochemistry: a Chemical Strategy for the Synthesis of Nanostructures. *Science* **1991**, *254*, 1312–1315. (b) Loo, Y.; Zhang, S.; Hauser, C. A. From Short Peptides to Nanofibers to Macromolecular Assemblies in Biomedicine. *Biotechnol. Adv.* **2012**, *30*, 593–603.

(7) Zhang, S. Fabrication of Novel Biomaterials through Molecular Self-Assembly. *Nat. Biotechnol.* **2003**, *21*, 1171–1178.

(8) Hamley, I. W. Peptide Fibrillization. *Angew. Chem., Int. Ed.* **2007**, *46*, 8128–8147.

(9) Rochet, J. C.; Lansbury, P. T. Amyloid Fibrillogenesis; Themes and Variations. *Curr. Opin. Struct. Biol.* **2000**, *10*, 60–68.

(10) (a) Harper, J. D.; Lansbury, P. T. Models of Amyloid Seeding in Alzheimer's Disease and Scrapie: Mechanistic Truths and Physiological Consequences of the Time-Dependent Solubility of Amyloid Proteins. *Annu. Rev. Biochem.* **1997**, *66*, 385–407. (b) Caughey, B.; Lansbury, P. T. Protofibrils, Pores, Fibrils, and Neurodegeneration: Separating the Responsible Protein Aggregates from the Innocent Bystanders. *Annu. Rev. Neurosci.* **2003**, *26*, 267–298.

(11) Goedert, M. Alpha-Synuclein and Neurodegenerative Diseases. *Nat. Rev. Neurosci.* **2001**, *2*, 492–501. Hamley, I. W. The Amyloid Beta Peptide: A Chemist's Perspective. Role in Alzheimer's and Fibrillization. *Chem. Rev.* **2012**, *112*, 5147–5192.

(12) (a) Wood, S. J.; Wetzel, R.; Martin, J. D.; Hurle, M. R. Prolines and Amylodoigenicity in Fragments of the Alzheimer's Peptide β/A4. *Biochemistry* **1995**, *34*, 724–730. (b) Findeis, M. A.; Musso, G. M.; Arico-Muendel, C. C.; Benjamin, H. W.; Hundal, A. M.; Lee, J. J.; Chin, J.; Kelley, M.; Wakefield, J.; Hayward, N. J.; et al. Modified-Peptide Inhibitors of Amyloid β-Peptide Polymerization. *Biochemistry* **1999**, *38*, 6791–6800. (c) Gordon, D. J.; Sciarretta, K. L.; Meredith, S. C. Inhibition of β-Amyloid(40) Fibrillogenesis and Disassembly of β-Amyloid(40) Fibrils by Short β-Amyloid Congeners Containing N-Methyl Amino Acids at Alternate Residues. *Biochemistry* **2001**, *40*, 8237–8245. (d) Fernandez-Escamilla, A.-M.; Rousseau, F.; Schymkowitz, J.; Serrano, L. Prediction and Sequence-Dependent Effects on the Aggregation of Peptides and Proteins. *Nat. Biotechnol.* **2004**, *22*, 1302–1306. (e) Rousseau, F.; Schymkowitz, J.; Serrano, L. Protein Aggregation and Amyloidosis: Confusion of the Kinds? *Curr. Opin. Struct. Biol.* **2006**, *16*, 118–126. (f) Lansbury, P. T.; Lashuel, H. A. A Century-Old Debate on Protein Aggregation and Neurodegeneration Enters the Clinic. *Nature* **2006**, *443*, 774–779.

(13) (a) Harper, J. D.; Wong, S. S.; Lieber, C. M.; Lansbury, P. T. Observation of Metastable Aβ Amyloid Protofibrils by Atomic Force Microscopy. *Chem. Biol.* **1997**, *4*, 119–125. (b) Harper, J. D.; Lieber, C. M.; Lansbury, P. T. Atomic Force Microscopy Imaging of Seeded Fibril Formation and Fiber Branching by the Alzheimer's Disease Amyloid β-Protein. *Chem. Biol.* **1997**, *4*, 951–959. (c) Bitan, G.; Kirkitadze, M. D.; Lomakin, A.; Vollers, S. S.; Benedeck, G. B.; Teplow, D. B. Amyloid β-Protein (Aβ) Assembly: Aβ40 and Aβ42 Oligomerize through Distinct Pathways. *Proc. Natl. Acad. Sci. U.S.A.* **2003**, *100*, 330–335.

(14) Smith, D. P.; Radford, S. E. Role of the Single Disulphide Bond of β_2-Microglobulin in Amyloidosis in Vitro. *Protein Sci.* **2001**, *10*, 1775–1784.

(15) Reeches, M.; Gazit, E. Formation of Closed-Cage Nanostructures by Self-Assembly of Aromatic Dipeptides. *Nano Lett.* **2004**, *4*, 581–585. Handelman, A.; Beker, P.; Amdursky, N.; Rosenman, G. Physics and Engineering of Peptide Supramolecular Nanostructures. *Phys. Chem. Chem. Phys.* **2012**, *14*, 6391–6408.

(16) Tracz, S. M.; Abedini, A.; Driscoll, M.; Rayleigh, D. P. Role of Aromatic Interactions in Amyloid Formation by Peptides Derived from Human Amylin. *Biochemistry* **2004**, *43*, 15901–15908.

(17) Kogiso, M.; Ohnishi, S.; Yase, K.; Masuda, M.; Shimizu, T. Self-Assembled Peptide Fibers from Valylvaline Bola-Amphiphiles by a Parallel β-Sheet Network. *Biochim. Biophys. Acta* **2000**, *1475*, 346−352.
(18) von Maltzahn, G.; Vauthey, S.; Santoso, S.; Zhang, S. Positively Charged Surfactant-Like Peptides Self-Assemble into Nanostructures. *Langmuir* **2003**, *19*, 4332−4337.
(19) (a) Hauser, C. A.; Deng, R.; Mishra, A.; Loo, Y.; Khoe, U.; Zhuang, F.; Cheong, D.; Accardo, A.; Sullivan, M.; Rickel, C.; et al. Natural Tri- to Hexapeptides Self-Assemble in Water to Amyloid {Beta}-Type Fiber Aggregates by Unexpected {Alpha}-Helical Intermediate Structures. *Proc. Natl. Acad. Sci. U.S.A.* **2011**, *108*, 1361−1366. (b) Mishra, A.; Loo, Y. H.; Deng, R. H.; Hee, H. T.; Ying, J. Y.; Hauser, C. A. Ultrasmall Natural Peptides Self-Assemble to Strong Temperature-Resistant Helical Fibers in Scaffolds Suitable for Tissue Engineering. *Nano Today* **2011**, *6*, 232−239.
(20) Würthner, F.; Kaiser, T. E.; Saha-Möller, C. R. J-Aggregates: From Serendipitous Discovery to Supramolecular Engineering of Functional Dye Materials. *Angew. Chem., Int. Ed.* **2001**, *50*, 3376−3410.
(21) Birks, J. B. Excimers. *Rep. Prog. Phys.* **1975**, *38*, 903−974.
(22) (a) Toniolo, C.; Crisma, M.; Bonora, G.; Benedetti, E.; Di Blasio, B.; Pavone, V.; Pedone, C.; Santini, A. Preferred Conformation of the Terminally Blocked $(Aib)_{10}$ Homo-Oligopeptide: A Long, Regular 3_{10}-Helix. *Biopolymers* **1991**, *31*, 129−138. (b) Karle, I. L.; Balaram, P. Structural Characteristics of α-Helical Peptide Molecules Containing Aib Residues. *Biochemistry* **1990**, *29*, 6747−6756.
(23) (a) Toniolo, C.; Peggion, C.; Crisma, M.; Formaggio, F.; Shui, X.; Eggleston, D. S. Structure Determination of Racemic Trichogin GA IV Using Centrosymmetric Crystals. *Nat. Struct. Mol. Biol.* **1994**, *1*, 908−914. (b) Benedetti, E.; Di Blasio, B.; Pavone, V.; Pedone, C.; Toniolo, C.; Crisma, M. Characterization at Atomic Resolution of Peptide Helical Structures. *Biopolymers* **1992**, *32*, 453−456.
(24) (a) Formaggio, F.; Bettio, A.; Moretto, V.; Crisma, M.; Toniolo, C.; Broxterman, Q. B. Disruption of the β-Sheet Structure of a Protected Pentapeptide, Related to the β-Amyloid Sequence 17−21, Induced by a Single, Helicogenic C^{α}-Tetrasubstituted α-Amino Acid. *J. Pept. Sci.* **2003**, *9*, 461−466. (b) Moretto, V.; Crisma, M.; Bonora, G. M.; Toniolo, C.; Balaram, H.; Balaram, P. Comparison of the Effect of Five Guest Residues on the β-Sheet Conformation of Host $(L\text{-}Val)_n$ Oligopeptide. *Macromolecules* **1989**, *22*, 2939−2944.
(25) Gilead, S.; Gazit, E. Inhibition of Amyloid Fibril Formation by Peptide Analogues Modified with α-Aminoisobutyric Acid. *Angew. Chem., Int. Ed.* **2004**, *43*, 4041−4044.
(26) Pispisa, B.; Stella, L.; Venanzi, M.; Palleschi, A.; Viappiani, C.; Polese, A.; Formaggio, F.; Toniolo, C. Quenching Mechanisms in Bichromophoric, 3_{10}-Helical Aib-Based Peptides, Modulated by Chain-Length Dependent Topologies. *Macromolecules* **2000**, *33*, 906−915.
(27) Kurana, R.; Coleman, C.; Inaescu-Zanetti, C.; Carter, S. A.; Krishna, V.; Grover, R. K.; Roy, R.; Singh, S. Mechanism of Thioflavin T Binding to Amyloid Fibrils. *J. Struct. Biol.* **2005**, *151*, 229−238.
(28) Laney, D. E.; Garcia, R. A.; Parsons, S. M.; Hansma, H. G. Changes in the Elastic Properties of Cholinergic Synaptic Vesicles as Measured by Atomic Force Microscopy. *Biophys. J.* **1997**, *72*, 806−813.
(29) van der Spoel, D.; Lindahl, E.; Hess, B.; Groenhof, G.; Mark, A. E.; Berendsen, H. J. C. GROMACS: Fast, Flexible and Free. *J. Comput. Chem.* **2005**, *26*, 1701−1718.
(30) Oostenbrinck, C.; Soares, T. A.; van der Veght, N. F.; van Gunsteren, W. F. Validation of the 53A6 GROMOS Force Field. *Eur. Biophys. J.* **2005**, *34*, 273−284.
(31) Birks, J. B. *Photophysics of Aromatic Molecules*; Wiley-Interscience: New York, 1970.
(32) Yao, H.; Domoto, K.; Isohashi, T.; Kimura, K. In Situ Detection of Birefringent Mesoscopic H and J Aggregates of Thiacarbocyanine Dye in Solution. *Langmuir* **2005**, *21*, 1067−1073.
(33) Uchida, K.; Tanaka, M.; Tomura, M. Excimer Emission of Crystalline Naphthalene. *J. Luminesc.* **1979**, *20*, 409−414.
(34) Ban, T.; Hamada, D.; Hasegawa, K.; Naiki, H.; Goto, Y. Direct Observation of Amyloid Fibril Growth Monitored by Thioflavine T Fluorescence. *J. Biol. Chem.* **2003**, *278*, 16462−16465.
(35) Winnik, F. M. Photophysics of Preassociated Pyrenes in Aqueous Polymer Solutions and in Other Organized Media. *Chem. Rev.* **1993**, *93*, 587−614.
(36) Stella, L.; Mazzuca, C.; Venanzi, M.; Palleschi, A.; Didoné, M.; Formaggio, F.; Toniolo, C.; Pispisa, B. Aggregation and Water-Membrane Partition as Major Determinants of the Activity of the Antibiotic Peptide Trichogin GA IV. *Biophys. J.* **2004**, *86*, 936−945.
(37) Marshall, K. E.; Morris, K. L.; Charlton, D.; O'Reilly, N.; Lewis, L.; Walden, H.; Serpell, L. C. Hydrophobic, Aromatic, and Electrostatic Interactions Play a Central Role in Amyloid Fibril Formation and Stability. *Biochemistry* **2011**, *50*, 2061−2071.
(38) Krimm, S.; Bandekar, J. Vibrational Spectroscopy and Conformation of Peptides, Polypeptides, and Proteins. *Adv. Protein Chem.* **1986**, *38*, 181−364.
(39) Pispisa, B.; Palleschi, A.; Stella, L.; Venanzi, M.; Mazzuca, C.; Formaggio, F.; Toniolo, C.; Broxtermann, Q. B. Effects of Helical Distortions on the Optical Properties of NH Amide Infrared Absorption in Short Peptides in Solution. *J. Phys. Chem. B* **2002**, *106*, 5733−5738.
(40) Kowalewski, T.; Holtzman, D. M. *In Situ* Atomic Force Microscopy Study of Alzheimer's {Beta}-Amyloid Peptide on Different Substrates: New Insights into Mechanism of {Beta}-Sheet Formation. *Proc. Natl. Acad. Sci. U.S.A.* **1999**, *96*, 3688−3693.
(41) Guo, S. L.; Akhremitchev, B. B. Investigation of Mechanical Properties of Insulin Crystals by Atomic Force Microscopy. *Langmuir* **2008**, *24*, 880−887.
(42) Guo, S. L.; Akhremitchev, B. B. Packing Density and Structural Heterogeneity of Insulin Amyloid Fibrils Measured by AFM Nanoindentation. *Biomacromolecules* **2006**, *7*, 1630−1636.
(43) Adamcik, J.; Mezzenga, R. Study of Amyloid Fibrils via Atomic Force Microscopy. *Curr. Opin. Colloid Interface Sci.* **2012**, *17*, 369−376.
(44) Smith, J. F.; Knowles, T. P. J.; Dobson, C. M.; Mac Phee, G. E.; Welland, M. E. Characterization of the Nanoscale Properties of Individual Amyloid Fibrils. *Proc. Natl. Acad. Sci.* **2006**, *103*, 15806−15811.
(45) Knowles, T. P. J.; Buehler, M. J. Nanomechanics of Functional and Pathological Amyloid Materials. *Nat. Nanotechnol.* **2011**, *6*, 469−479.
(46) Sunde, M.; Blake, C. C. F. From the Globular to the Fibrous State: Protein Structure and Structural Conversion in Amyloid Formation. *Q. Rev. Biophys.* **1998**, *31*, 1−39.
(47) (a) Conway, K. A.; Lee, S. J.; Rochet, J. C.; Ding, T. T.; Williamson, R. E.; Lansbury, P. T. Acceleration of Oligomerization, not Fibrillization, is a Shared Property of Both α-Synuclein Mutations Linked to Early-Onset Parkinson's Disease: Implications for Pathogenesis and Therapy. *Proc. Natl. Acad. Sci. U.S.A.* **2000**, *97*, 571−576. (b) Kayed, R.; Head, E.; Thompson, J. L.; McIntire, T. M.; Milton, S. C.; Cotman, C. W.; Glabe, C. G. Common Structure of Soluble Amyloid Oligomers Implies Common Mechanism of Pathogenesis. *Science* **2003**, *300*, 486−489. (c) Cleary, J. P.; Walsh, D. M.; Hopfmesister, J. J.; Shankar, G. M.; Kuskowski, M. A.; Selkoe, D. J.; Ashe, K. H. Natural Oligomers of the Amyloid-β Protein Specifically Disrupt Cognitive Function. *Nat. Neurosci.* **2005**, *8*, 79−84.
(48) Sunde, M.; Blake, C. C. F. The Structure of Amyloid Fibrils by Electron Microscopy and X-Ray Diffraction. *Adv. Protein Chem.* **1997**, *50*, 123−159.
(49) Zavyalova, E. G.; Protopopova, A. D.; Kopylov, A. M.; Yaminski, I. V. Investigation of Early Stages of Fibrin Association. *Langmuir* **2011**, *27*, 4922−4927.
(50) (a) Gazit, E. A Possible Role for π-Stacking in the Self-Assembly of Amyloid Fibrils. *FASEB J.* **2002**, *16*, 77−83. (b) Gazit, E. Self-Assembly of Short Aromatic Peptides into Amyloid Fibrils and Related Nanostructures. *Prion* **2007**, *1*, 32−35.
(51) Mahler, A.; Reches, M.; Rechter, M.; Cohen, S.; Gazit, E. Rigid, Self-Assembled Hydrogel Composed of a Modified Aromatic Dipeptide. *Adv. Mater.* **2006**, *18*, 1365−1370.

(52) Marek, P.; Abedini, A.; Song, B.; Kanungo, M.; Johnson, M. E.; Gupta, R.; Zaman, W.; Wong, S. S.; Raleigh, D. P. Aromatic Interactions Are not Required for Amyloid Fibril Formation by Islet Amyloid Polypeptide but Do Influence the Rate of Fibril Formation and Fibril Morphology. *Biochemistry* **2007**, *46*, 3255−3261.
(53) (a) Chen, L.; Morris, K.; Laybourn, A.; Elias, D.; Hicks, M. R.; Rodger, A.; Serpell, L.; Adams, D. J. Self-Assembly Mechanism for a Naphthalene-Dipeptide Leading to Hydrogelation. *Langmuir* **2010**, *26*, 5232−5242. (b) Chen, L.; Revel, S.; Morris, K.; Serpell, L. C.; Adams, D. J. Effect of Molecular Structure on the Properties of Naphthalene-Dipeptide Hydrogelators. *Langmuir* **2010**, *26*, 13466−13471.
(54) Aggeli, A.; Nyrkova, I. A.; Bell, M.; Harding, R.; Carrick, L.; McLeish, T. C. B.; Semenov, A. N.; Boden, N. Hierarchical Self-Assembly of Chiral Rod-Like Molecules as a Model for Peptide β-Sheet Tapes, Ribbons, Fibrils, and Fibers. *Proc. Natl. Acad. Sci. U.S.A.* **2001**, *98*, 11857−11862.
(55) Jimenez, J. L.; Nettleton, E. J.; Bouchard, M.; Robinson, C. V.; Dobson, C. M.; Saibil, H. R. The Protofilament Structure of Insulin Amyloid Fibrils. *Proc. Natl. Acad. Sci. U.S.A.* **2002**, *99*, 9196−9201.